

# Renal epithelial miR-205 expression correlates with disease severity in a mouse model of congenital obstructive nephropathy

Michael E. Wilhide<sup>1</sup>, James D. Feller<sup>1</sup>, Birong Li<sup>1</sup>, Ahmad Z. Mohamed<sup>2</sup>, Brian Becknell<sup>1,3</sup>, Ashley R. Jackson<sup>4</sup>, Kirk M. McHugh<sup>4</sup> and Susan E. Ingraham<sup>1,3</sup>

**BACKGROUND:** Congenital obstructive nephropathy (CON) is a leading cause of pediatric chronic kidney disease (CKD). Despite optimal surgical and medical care, there is a high rate of CKD progression. Better understanding of molecular and cellular changes is needed to facilitate development of improved biomarkers and novel therapeutic approaches in CON.

**METHODS:** The *megabladder* (*mgb*) mouse is an animal model of CKD with impaired bladder emptying, hydronephrosis, and progressive renal injury. In this study, we characterize a particular microRNA, miR-205, whose expression changes with the degree of hydronephrosis in the *mgb*<sup>-/-</sup> kidney.

**RESULTS:** Expression of miR-205 is progressively increased in the adult *mgb*<sup>-/-</sup> mouse with worsening severity of hydronephrosis. miR-205 expression is correlated with altered expression of cytokeratins and uroplakins, which are markers of cellular differentiation in urothelium. We describe the spatial pattern of miR-205 expression, including increased expression in renal urothelium and novel miR-205 expression in medullary collecting duct epithelium in the congenitally obstructed kidney.

**CONCLUSION:** miR-205 is increased with severity of CON and CKD in the *mgb*<sup>-/-</sup> mouse and may regulate urothelial differentiation.

Chronic kidney disease (CKD) is characterized by the gradual loss of kidney function over time. It is the common end result of a wide range of diseases and processes that cause permanent damage and scarring to the kidney. Congenital obstructive nephropathy (CON), a leading cause of pediatric CKD, is a complex disease process characterized by pathological changes in kidney development and function resulting from restriction of antegrade urine flow beginning *in utero* (1,2). Pre- or postnatal surgical interventions may alter the rate of decline in renal function, but in many patients CKD progression is inevitable (3). Up to 70% of children with CKD due to CON will progress to end-stage renal disease by

20 y of age, resulting in a 10-y survival rate of approximately 80% and an age-specific mortality rate 30 times that seen in children without end-stage renal disease (4). The direct link between obstructed urine flow beginning *in utero* and abnormal renal development and function represents a central paradigm of urogenital pathogenesis that has far-reaching clinical implications.

Animal models of obstructive nephropathy have utilized both surgical and genetic approaches. We have previously characterized the pathogenesis of CON in the *megabladder* (*mgb*) mouse (5,6). The *mgb* mouse is a unique transgene-induced mutant mouse line in which impaired bladder emptying and hydronephrosis are prominent features (7,8). The CKD course followed by male *mgb*<sup>-/-</sup> mice, from *in utero* voiding impairment to end-stage renal disease and death at sexual maturation, provides an excellent opportunity to investigate the molecular and cellular factors that drive the onset and progression of CON.

A rapidly expanding body of literature documents the critical role that microRNAs (miRs) play in renal physiology and pathology (9–12). miRs are short endogenous noncoding RNA molecules that regulate the expression of genes through mRNA cleavage, translational repression, or translational activation. miRs are extremely important gene regulators, controlling key cell functions such as developmental switching, cell differentiation, cell proliferation, and apoptosis. miRs are known to play a role in the regulation of kidney homeostasis, kidney development, and in various kidney disease, including fibrotic kidney disease (10), although they have not previously been investigated in CON.

miR-205 has been identified as an epithelial-specific master regulator in multiple tissues, involved in both normal development and pathological states including cancer (13–16). Studies have suggested a critical role for miR-205 in several types of kidney diseases, including both glomerular and tubular disorders (17–19). miR-205 is also the most-upregulated miR in the unilateral ureteral obstruction mouse model of obstructive renal fibrosis (20).

<sup>1</sup>Center for Clinical and Translational Research, The Research Institute at Nationwide Children's Hospital, Columbus, Ohio; <sup>2</sup>Department of Urology, University of Louisville, Louisville, Kentucky; <sup>3</sup>Department of Pediatrics, The Ohio State University, Columbus, Ohio; <sup>4</sup>Center for Molecular and Human Genetics, The Research Institute at Nationwide Children's Hospital, Columbus, Ohio. Correspondence: Susan E. Ingraham ([susaneingraham@gmail.com](mailto:susaneingraham@gmail.com))

Received 9 March 2016; accepted 7 April 2016; advance online publication 6 July 2016. doi:10.1038/pr.2016.121

In this study, we examine the association of miR-205 expression patterns with the degree of hydronephrosis in the *mgb*<sup>-/-</sup> kidney, describe spatial and cellular patterns of miR-205 expression in the normal and the obstructed kidney, identify altered patterns of expression of urothelial differentiation markers that correlate with miR-205, and discuss potential roles of miR-205 in the pathogenesis of CON and CKD in this established animal model.

## RESULTS

### miR-205 Expression Increases During Maturation and Progression of Hydronephrosis in *mgb*<sup>-/-</sup> Mice

miR-205 is present during kidney development from embryonic day 15.5 (E15.5) through birth (day 0 to day 1), but the differences in expression levels between *mgb*<sup>-/-</sup> and wild-type (WT) kidneys are either small (no >1.3-fold) or not statistically significant (Figure 1). Quantitative reverse transcription PCR (RT-PCR) demonstrated that relative expression of mature miR-205 is significantly upregulated in weanling (3.1-fold) and adult (3.5-fold) *mgb*<sup>-/-</sup> kidneys compared with WT. In the adults, the level of miR-205 expression correlates with the degree of hydronephrosis (Figure 2). We found a significant proportional increase in relative miR-205 expression when the data were stratified by severity of hydronephrosis (Figure 2e: mild, 1.3-fold increase relative to WT, not statistically significant; moderate, 2.4-fold increase,  $P = 0.02$ ; severe: 5.3-fold,  $P = 0.004$ ; Kruskal–Wallis equality-of-populations rank test across

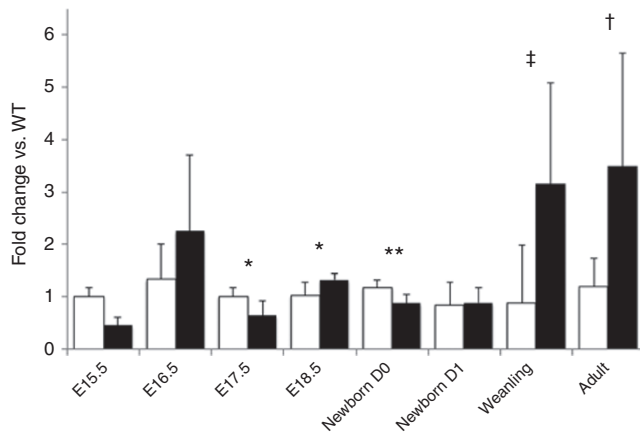


**Figure 1.** Timeline of renal miR-205 expression during development and progression of hydronephrosis in the *mgb*<sup>-/-</sup> mouse. Reverse transcription PCR (RT-PCR) results from a panel of male megabladder (*mgb*<sup>-/-</sup>) kidney samples spanning developmental and chronic kidney disease progression stages from embryonic day 15.5 (E15.5) through adulthood. miR-205 expression is indicated relative to mean miR-205 expression in age-matched wild-type (WT) kidneys. Time points include embryonic day 15.5 (E15.5), E16.5, E17.5, E18.5, newborn day 0 (D0), day 1 (D1), weanling (day 20–22), and adult (4–5 wk including all degrees of hydronephrosis). Fold change is relative to WT and represents the mean  $\pm$  SD with three independent RT-PCR runs of three technical replicates per run, normalized to sno234. White, WT; black, *mgb*<sup>-/-</sup>. Number of animals ( $n$ ) per group, E15.5: WT  $n = 4$ , *mgb*<sup>-/-</sup>  $n = 5$ . E16.5: WT  $n = 5$ , *mgb*<sup>-/-</sup>  $n = 5$ . E17.5: WT  $n = 4$ , *mgb*<sup>-/-</sup>  $n = 5$ . E18.5: WT  $n = 5$ , *mgb*<sup>-/-</sup>  $n = 5$ . D0: WT  $n = 9$ , *mgb*<sup>-/-</sup>  $n = 4$ . D1: WT  $n = 4$ , *mgb*<sup>-/-</sup>  $n = 5$ . Weanling: WT  $n = 11$ , *mgb*<sup>-/-</sup>  $n = 9$ . Adult: WT  $n = 6$ , *mgb*<sup>-/-</sup>  $n = 18$ . The  $P$  values resulting from Mann–Whitney test are indicated: \* $P = 0.05$ ; \*\* $P = 0.02$ ; † $P = 0.01$ ; †† $P = 0.006$ . If no symbol is shown, result was not statistically significant ( $P > 0.05$ ).

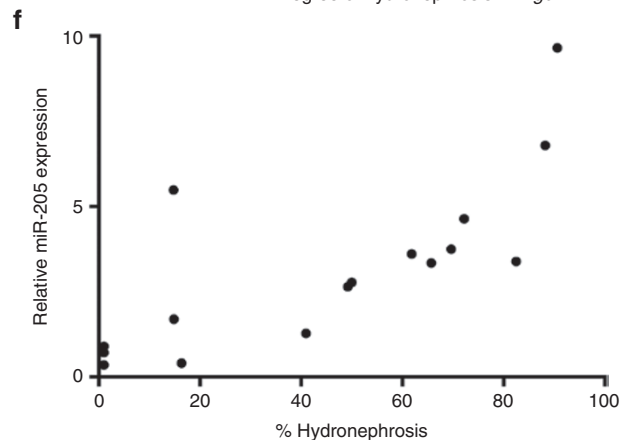
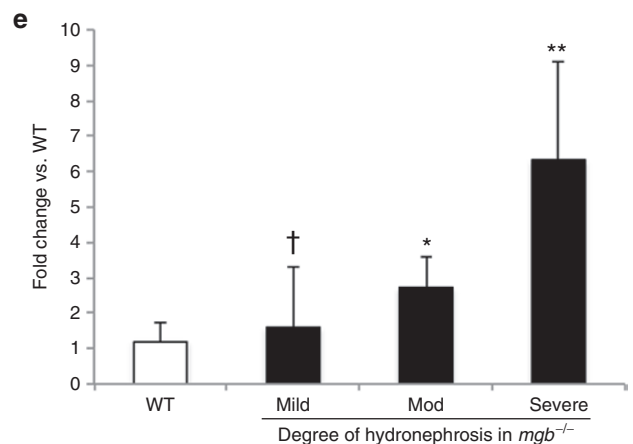
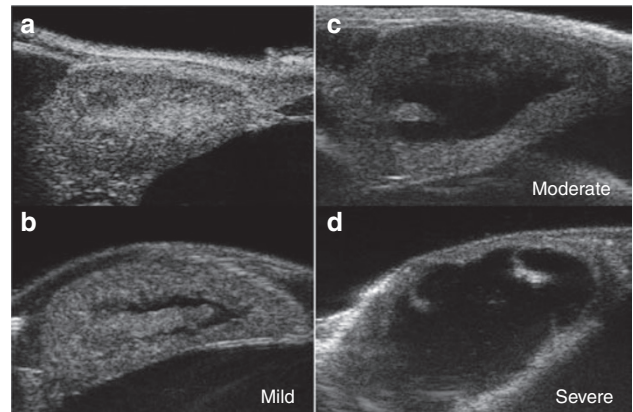


**Figure 2.** miR-205 expression correlates with degree of hydronephrosis in *mgb*<sup>-/-</sup> adults. (a–d) Kidney cross-sectional ultrasound showing representative examples of hydronephrosis stratification in adult *mgb*<sup>-/-</sup> kidneys: (a) no hydronephrosis (0% of anterior–posterior line crosses fluid in the renal pelvis), (b) mild hydronephrosis (8%), (c) moderate hydronephrosis (45%), and (d) severe hydronephrosis (81%). (e) Stratification of the adult *mgb*<sup>-/-</sup> population from Figure 1 by severity of hydronephrosis compared with wild type (WT). Pairwise comparisons of group means were performed using the Mann–Whitney test, with resulting  $P$  values shown by crosses for comparison with WT and asterisks for comparison to severe group. † $P = 0.01$ ; \* $P = 0.02$ ; \*\* $P = 0.004$ . If no symbol is shown, result was not statistically significant ( $P > 0.05$ ). Fold change is relative to WT kidneys and represents the mean  $\pm$  SD with three independent reverse transcription PCR runs of three technical replicates per run, normalized to sno234. Number of animals ( $n$ ) per group, WT  $n = 6$ , Mild  $n = 7$ , Mod  $n = 5$ , Severe  $n = 6$ . (f) Correlation of relative miR-205 expression with measurement of degree of hydronephrosis in kidney cross-sectional 2D ultrasound images using the method of Carpenter *et al.* (40). Spearman rho = 0.78,  $P = 0.0003$ .

all three *mgb*<sup>-/-</sup> severity groups, *P* = 0.003). High positive correlation (Spearman rho = 0.78) was found between relative miR-205 expression by RT-PCR and the degree of hydronephrosis

as measured in kidney cross-sectional 2D ultrasound images (Figure 2f). Stratification by severity of hydronephrosis at the weanling stage was not possible due to small numbers of animals with greater than mild hydronephrosis. Of note, wide variability in expression was seen in both *mgb*<sup>-/-</sup> and WT kidneys at the weanling stage, suggesting that miR-205 fluctuations at this age may be in part a developmental rather than disease-related observation.

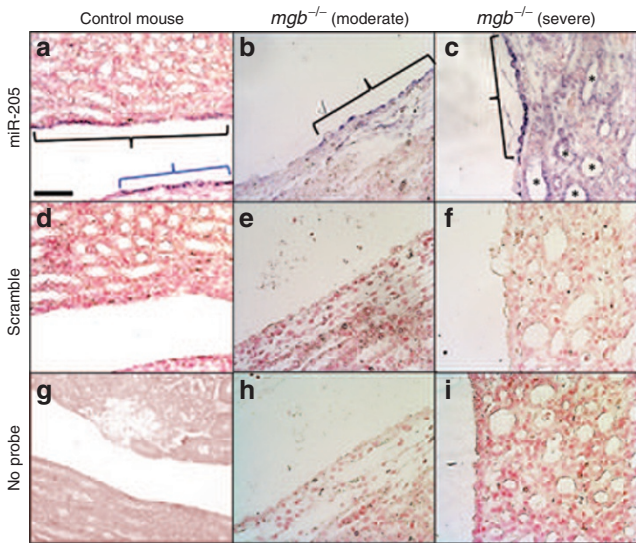


**Figure 3.** miR-205 expression in the medulla of wild-type (WT) and *mgb*<sup>-/-</sup> kidneys. *In situ* hybridization of a miR-205-specific probe demonstrates the expression of miR-205 in the renal pelvic urothelium (black brackets) of (a) normal WT, (b) moderately hydronephrotic, or (c) severely hydronephrotic *mgb*<sup>-/-</sup> kidneys. Staining (purple) intensifies with increasing severity of hydronephrosis. Positive staining can also be seen in the epithelium lining the renal papilla (a, blue bracket) and in the epithelium of dilated medullary tubular structures in the severely affected kidney (c, asterisks). Corresponding kidney sections hybridized with a scrambled miRNA probe (d–f) or no probe (g–i) show no staining. Bar in panel A = 50 μm and gives scale for all images. 40× objective.

**miR-205 Is Expressed in the Renal Urothelium in WT and *mgb*<sup>-/-</sup> Kidneys**

We next evaluated the source of the increased renal miR-205 expression in hydronephrotic *mgb*<sup>-/-</sup> kidneys by *in situ* hybridization (ISH). In the WT adult mouse, the only renal compartment where miR-205 expression is detected is the epithelium overlying the medulla and renal papilla (Figure 3a). There appears to be a shift from basolateral to more apical or diffuse subcellular distribution in the *mgb*<sup>-/-</sup> kidney, with miR-205 expression visibly intensified in the urothelium of kidneys from severely hydronephrotic *mgb*<sup>-/-</sup> mice (Figure 3b,c). In the *mgb*<sup>-/-</sup> kidney, urothelial miR-205 expression is primarily within the basal layer (Figure 4, top). Beyond the ureteropelvic junction, however, miR-205 is more evenly distributed through all urothelial cell layers (Figure 4, bottom).

**Novel Expression of miR-205 Occurs in Dilated Collecting Ducts in CON**

We found novel expression of miR-205 in collecting ducts of severely hydronephrotic *mgb*<sup>-/-</sup> kidneys that is absent in WT or less severely affected *mgb*<sup>-/-</sup> kidneys. miR-205 is expressed in the epithelium of dilated tubular structures within the

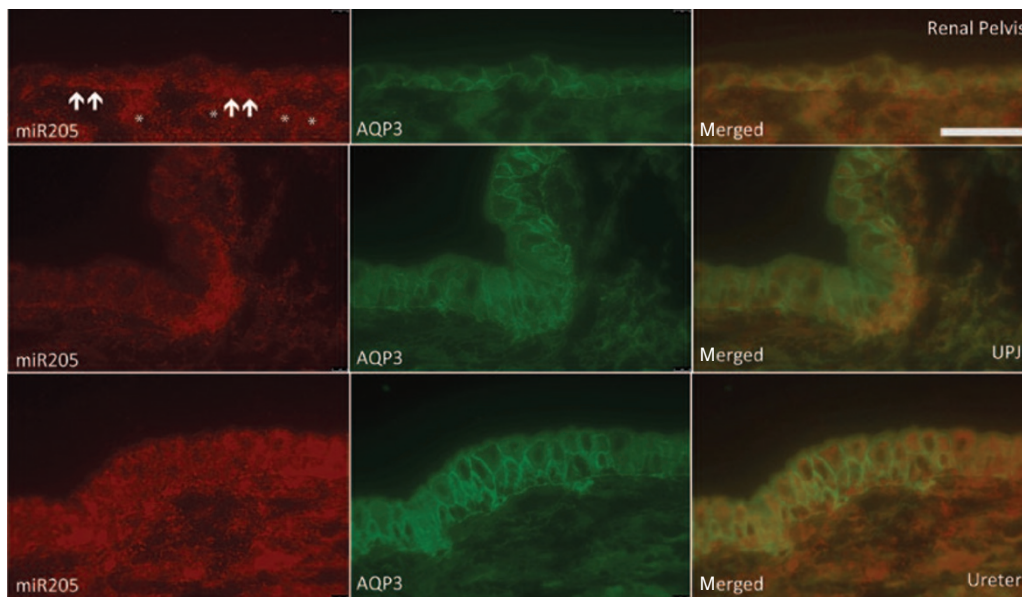


**Figure 4.** miR-205 is expressed in the basal layer of the renal pelvis urothelium in the *mgb*<sup>-/-</sup> mouse model of congenital obstructive nephropathy. (top) *In situ* hybridization (ISH) of kidney from a 33-d-old female *mgb*<sup>-/-</sup> mouse with bilateral severe hydronephrosis using a miR-205-specific probe shows miR signal in the urothelium (arrows) and in nearby collecting ducts (asterisks). Combined ISH–immunohistochemistry with an anti-aquaporin 3 (Aqp3) antibody delineates the two urothelial cell layers and identifies miR-205 predominantly in the basal layer. (middle) A similar localization to the basal layer of urothelium is found at the ureteropelvic junction (UPJ; white arrows). (bottom) Within the ureter, miR-205 expression is more uniform throughout the urothelial cell layers. Bar = 50 μm. 40× objective.

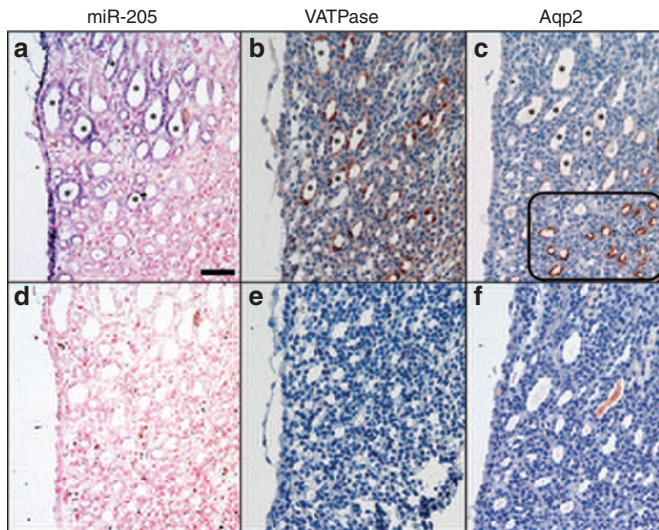


**Figure 5.** Immunohistochemistry with anti-V-ATPase and anti-AQP2 identifies the dilated tubular structures expressing miR-205 as collecting ducts that have lost AQP2 expression. (a) miR-205-positive dilated tubular structures (asterisks) in the inner medulla of a severely affected *mgb*<sup>-/-</sup> kidney. (b) Dilated tubules in this region also stain positively with a V-ATPase-specific antibody in the same mouse kidney. (c) Little or no signal is detected in this region with an AQP2-specific antibody although nearby normal-caliber collecting ducts (box) are positive for AQP2. Controls with a scrambled RNA probe (d) and with no primary antibody (e,f) confirm that staining is specific. Bar in panel A = 50  $\mu$ m and gives scale for all images. 20 $\times$  objective.

inner medulla (Figure 3c, asterisks). These miR-205-positive structures are observed only in severely hydronephrotic *mgb*<sup>-/-</sup> kidneys, where dilated and/or atrophic collecting ducts are frequently seen. No miR-205 is detected within the inner medulla of WT kidneys or moderately hydronephrotic *mgb*<sup>-/-</sup> kidneys (Figure 3a,b). Intense staining of distinct cells in these structures by an antibody to vacuolar ATPase (V-ATPase (21); Figure 5) verifies that these miR-205-positive structures are medullary collecting ducts. These dilated collecting ducts, however, have lost expression of aquaporin 2 (AQP2 (22); Figure 5c).

#### miR-205 Is Activated in Multiple Cell Types in Dilated Collecting Ducts in the *mgb*<sup>-/-</sup> Mouse Kidney

We performed ISH for miR-205 and immunohistochemistry for the intercalated cell marker V-ATPase and the principal cell marker AQP2 on serial sections to identify the specific cell type(s) expressing miR-205 in the dilated collecting ducts in severely hydronephrotic *mgb*<sup>-/-</sup> kidneys (Figure 6). As suggested by the frequent circumferential staining of these structures with miR-205 seen at low power (Figure 5a), miR expression appears to be induced in multiple cell types. In some collecting ducts, overlap of miR-205 distribution with the intense V-ATPase expression characteristic of intercalated cells is seen (Figure 6f,i). The presence of miR-205 in principal cells is more difficult to verify, because expression of specific markers such as AQP2 is lost in many of the atrophic, dilated ducts that express miR-205. However, rare collecting ducts co-expressing miR-205 and AQP2 were observed and indicate

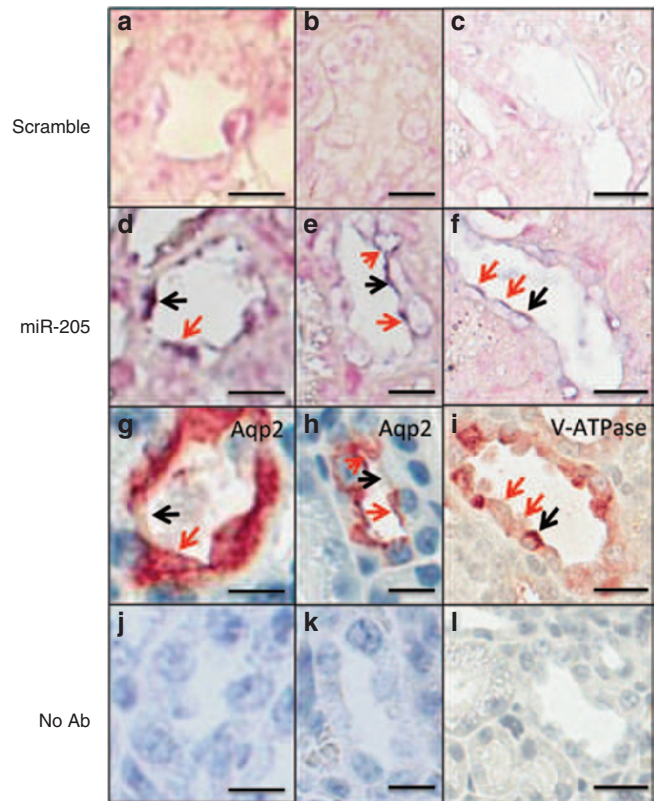


**Figure 6.** High-power images of miR-205, V-ATPase, and AQP2 expression. Serial sections from severely hydronephrotic adult *mgb*<sup>-/-</sup> kidneys were probed with (a–c) a nonspecific (scramble) RNA probe, (d–f) a miR-205-specific RNA probe, (g,h) antibody to aquaporin 2 (AQP2), and (i) antibody to V-ATPase. Negative control for immunohistochemistry is shown in panels (j–l) (No Ab). Arrows indicate miR-205 positive cells (d–f) and the corresponding locations on immunohistochemistry sections (g–i). A red arrow indicates a principal cell (AQP2-positive or V-ATPase-negative). A black arrow indicates an intercalated cell (V-ATPase positive or AQP2 negative). Bar = 10  $\mu$ m. 40 $\times$  objective.

the presence of both molecules in the same principal cells (Figure 6d,e,g,h). Combined ISH–immunohistochemistry with fluorescent detection on single sections was attempted to confirm colocalization (as in Figure 4), but could not be interpreted due to high background (data not shown).

#### Expression of Tight Junction Proteins in *mgb* Mouse Kidneys

Tight junction proteins have been reported as targets of miR-205 in bladder urothelium (23). We performed RT-PCR and western blotting to investigate whether these same targets are affected by miR-205 expression in the *mgb* kidney. No significant changes in *Cgln1*, *Tjp1*, or *Cdc42* were observed at the mRNA or protein level when whole kidney was analyzed (data not shown).

#### Expression of Urothelial Differentiation Markers Correlates With miR-205 Upregulation

Silencing of miR-205 in cultured bladder epithelial cells has previously been shown to alter the expression patterns of cytokeratins and uroplakins (23). Cytokeratins (*Krt*)5, 8, 14, 18, 19, 20 and Uroplakins (*Upk*)1a and 1b are significantly increased in

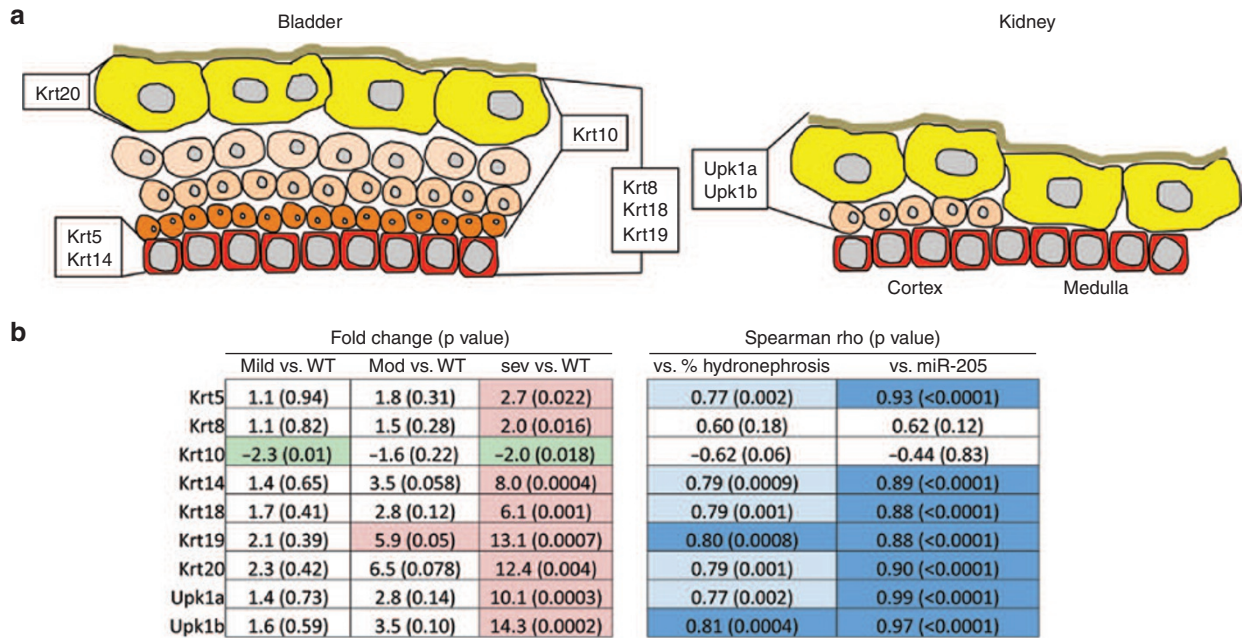


**Figure 7.** The expression of cytokeratins and uroplakins is altered in severely affected *mgb*<sup>-/-</sup> kidneys and strongly correlates with miR-205 levels. (a) Schematic of urothelial organization in the bladder (left) and kidney (right). The previously reported cytokeratin (Krt) and uroplakin (Upk) profiles of basal (red), intermediate (orange), and superficial (yellow) bladder cells and the urothelial plaque (tan) are depicted. For simplicity and clarity, Krt distribution is shown on the left and Upk on the right, but these markers are present in both organs. (b) Relative expression levels and correlation of cytokeratins and uroplakins in *mgb*<sup>-/-</sup> kidneys with mild, moderate (mod), and severe (sev) hydronephrosis. Groups reaching statistical significance ( $P \leq 0.05$ ) for expression change are indicated with pink (increased relative to wild type) or green (decreased) shading. Spearman correlation to both % hydronephrosis and miR-205 level are shown. Shading indicates strong ( $0.6 \leq \rho \leq 0.79$ ; light blue) or very strong ( $\rho \geq 0.8$ ; darker blue) correlation with Bonferroni-adjusted  $P \leq 0.05$ .

severely affected *mgb*<sup>-/-</sup> kidneys compared with WT (Figure 7). *Krt10* expression is decreased in *mgb*<sup>-/-</sup> kidneys. *Krt5*, *Krt14*, *Krt18*, *Krt 19*, *Krt20*, *Upk1a*, and *Upk1b* are each strongly correlated with degree of hydronephrosis and very strongly correlated with expression of miR-205 (Figure 7). *Krt10* demonstrates a weaker negative correlation with hydronephrosis, but no correlation with miR-205.

**DISCUSSION**

In this study, we demonstrated that miR-205 expression progressively increases with increasing severity of hydronephrosis in the *mgb*<sup>-/-</sup> model of CON and CKD. We localized miR-205 expression to the renal urothelium and epithelial cells in dilated collecting ducts. miR-205 expression strongly correlates with expression of uroplakins and cytokeratins that are markers of urothelial differentiation.

In the mouse, the definitive (metanephric) kidneys begin to form around embryonic day 10.5 (E10.5). In contrast to human kidney development, nephrogenesis is still active at birth in the mouse, continuing until 7–10 d postnatally. In *mgb*<sup>-/-</sup> mice, bladder smooth muscle development is severely impaired (8). As a result of impaired antegrade urine flow, hydroureteronephrosis develops with variable timing and severity, arising as early as E17.5 and often progressing throughout the lifetime of the animal (5,6).

In the embryonic mouse kidney, miR-205 has been previously reported at low expression levels at E18.5 by one group (24) but absent in embryonic kidneys in a different mouse

model (25). However, the second group only examined miR-205 in the kidney globally, not in renal urothelium specifically (R. Yi, personal communication). Our results demonstrate that prior to the development of significant hydronephrosis during the first weeks after birth, miR-205 is expressed with little or no difference in levels between *mgb*<sup>-/-</sup> and WT mice. In adult *mgb*<sup>-/-</sup> mice, miR-205 expression progressively increases with worsening severity of hydronephrosis. Other studies have also found a correlation between miR-205 and disease severity in CKD. miR-205 is increased in patients with hypertensive nephrosclerosis (19) and in primary tubular cells from patients with autosomal dominant polycystic kidney disease (26). miR-205 correlates with degree of proteinuria in primary focal segmental glomerulosclerosis (17) and with estimated glomerular filtration rate and degree of tubulointerstitial scarring in IgA nephropathy (18). Our study implicates miR-205 in the response to renal pelvic distention. In contrast to the human megaureter–megacystis syndrome in which vesicoureteral reflux is a prominent feature (27,28), we have not found urinary reflux to be significant in the pathophysiology of the *mgb*<sup>-/-</sup> mouse (data not shown). We therefore conclude that the altered miR-205 expression is a consequence of the chronic downstream impairment of urine flow.

Our analysis of the spatial distribution of miR-205 within the kidney demonstrated modest expression in the renal urothelium in normal adult mice. As the renal pelvis becomes distended in the obstructed *mgb*<sup>-/-</sup> kidney, miR-205 expression increases. miR-205 expression is also induced in the epithelium

of dilated inner medullary collecting ducts. Affected tubules expressing miR-205 frequently lack expression of AQP2, a water channel that plays a critical role in controlling water permeability in the collecting ducts as the target for vasopressin (29). The mutually exclusive expression of miR-205 and AQP2 in collecting ducts is unlikely to be the result of direct regulation of *Aqp2* by miR-205, as no miR-205 seed sequence can be found in the murine *Aqp2* transcript (data not shown). Of note, the structures where we found miR-205 consistently activated in obstruction are derived from the ureteric bud and represent the most distal portions of the urine collecting system in the kidney.

Previously reported and hypothesized functions of miR-205 in other diseases and models are illuminating to understanding the role miR-205 may play in the renal urothelium and distal nephron in CON. In cancer, miR-205 is a key regulator of the potential for epithelial growth and differentiation. Expression studies in a variety of tumor types suggest that miR-205 is expressed at increased levels in subtypes with more benign epithelial characteristics and decreased levels in more aggressive and invasive subtypes (30). In different contexts, miR-205 can either promote or suppress tumorigenesis, activating or maintaining the epithelial phenotype and directing cell fate decisions (31). A role of miR-205 in regulating the urothelial phenotype is suggested by its increased expression in upper urinary tract urothelial cancers (32) and its ZEB1/2-dependent regulation of epithelial-to-mesenchymal transition in bladder cancer cells (33). In bladder urothelium, miR-205 may regulate multiple tight junction–related proteins in the undifferentiated basal and intermediate cell layers. Overexpression of miR-205 in Madin-Darby canine kidney (MDCK) cells actually prevents tight junction formation, and miR-205 silencing in primary cultured bladder urothelium increases expression of specific tight junction proteins and has significant effects on expression of cytokeratins and uroplakins (23). Thus, miR-205 participates in regulation of urothelial differentiation and function. In the structurally and functionally similar stratified epithelium of skin, miR-205 has a critical role in epithelial regeneration by promoting the proliferation and expansion of skin cell progenitors (34). Under oxidative stress in the proximal renal tubule, miR-205 may serve to protect against a maladaptive, injurious response to reoxygenation (35).

In the congenitally obstructed kidney, we see a profound effect on the expression of cytokeratins and uroplakins, although the expression profile of these urothelial markers in the obstructed kidney *in vivo* is distinct from that reported in bladder cells *in vitro*. Cultured bladder urothelium responds to miR-205 silencing by increasing expression the simple keratins *Krt8*, *Krt18*, *Krt19*, and *Krt20* as well as the urothelial differentiation products *Upk1a* and *Upk1b*, and decreasing expression of the basal cell keratins *Krt5* and *Krt14* (23). Of note, miR-205 also positively correlates with *Krt5*, *Krt14*, *Krt15*, and *Krt17* in normal and cancerous prostate tissue (36). In the *mgb*<sup>-/-</sup> mouse kidney, we observe increased expression of *Krt5* and *Krt14* very strongly correlated to miR-205 expression levels, as expected

from the previously published data. However, we also observe miR-205-associated increases in several simple keratins (*Krt18*, *Krt19*, *Krt20*) as well as *Upk1a* and *Upk1b*, contradictory to what the *in vitro* bladder cell study demonstrated. The difference in response of the simple cytokeratins could be explained by the inclusion of cytokeratin-expressing renal tubular cells in our whole kidney tissue samples. However, *Upk1a* and *1b* are highly specific markers for differentiated urothelium. There is no predicted miR-205 binding site in the 3′ untranslated region of any of the uroplakins or keratins studied, so there are likely intermediate signals between miR-205 and these downstream targets; these intermediaries may differ between bladder and kidney, or between *in vitro* and *in vivo* model systems. Bladder and kidney urothelium are morphologically distinct (see Figure 7, top) and have different embryological origins—the bladder urothelium is endoderm-derived, and the kidney urothelium is mesoderm-derived as a product of the ureteric bud. Additional investigation is needed to identify the intermediate factors in miR-205 regulation of urothelial differentiation and determine the cause of this apparent contradiction in the urothelial response to miR-205. Our analysis failed to show any significant alteration in expression of tight junction–associated proteins. More detailed functional and structural studies are needed to determine the fate of tight junctions in the obstructed kidney.

In the kidney, miR-205 likely plays a protective and adaptive role, helping to defend critical epithelial layers of the urothelium and collecting duct from the mechanical stress and physiological consequences of renal distention and urine stasis, as well as promoting cellular regeneration. Other *in vivo* models of antenatal obstruction such as the fetal nonhuman primate model of unilateral ureteric obstruction have demonstrated significant medullary changes including epithelial–mesenchymal transition of intercalated cells and cellular migration that results in formation of peritubular collars, a change that would enhance structural integrity although with probable detrimental effects on nephrogenesis and growth (37).

We previously proposed a model of renal adaptation in the *mgb*<sup>-/-</sup> mouse model centered on a critical balance between tissue remodeling and renal pathogenesis (7). We postulated that increasing distention and pressure within the renal pelvis cause the gradual expansion and proliferation of the renal urothelium, producing significant changes in the structure, function, and permeability of the urothelial membrane. This study supports a role of miR-205 in regulation of urothelial differentiation, providing a potential mechanism for these changes. In our revised model, worsening hydronephrosis induces expression of miR-205, which may mediate an adaptive response (8) that alters or reactivates urothelial differentiation pathways. Although these changes may have some deleterious effects due to altered urothelial function and permeability, they may be critical in initiating an organ-protective response during pathogenic insult to the kidney.

In addition to distending pelvic urothelium, obstruction leads to tubular dilatation and transmission of increased hydrostatic pressure backward along the length of the nephron.

This could trigger miR-205 signaling pathways in the collecting duct epithelium, where cytokeratins are also known to play critical roles (38,39). It is thus intriguing to speculate that miR-205 plays a central role in epithelial regeneration, proliferation, and/or adaptation in multiple renal cell types in response to congenital obstruction.

## METHODS

### Animal Model

This study was performed with approval from the Institutional Animal Care and Use Committee of Nationwide Children's Hospital. Age and sex-matched FVB/N were used as WT controls. *mgb<sup>-/-</sup>* animals were genotyped as previously described (6). Grading of hydronephrosis was based on measuring the proportions of renal parenchyma vs. fluid-distended renal pelvis in kidney cross-sectional 2D ultrasound images as previously described (40), with each kidney being stratified into mild, moderate, or severe categories. This method does not directly correlate with clinical grading scales of hydronephrosis such as the Society of Fetal Urology hydronephrosis grading system, which cannot be reliably applied to mice due to the unilobar structure of the mouse kidney and consequent absence of calyces.

### RNA Isolation

Total RNA including the small RNA fraction was isolated from snap-frozen kidney samples at specific developmental time points: E15.5, E16.5, E17.5, E18.5, immediate newborn (day 0), recent newborn (day 1), weanling (20–22 d), and adult (4–5 wk), using the TissueLyser II (Qiagen USA, Valencia, CA) and mirVana miRNA isolation kit (ThermoFisher Scientific, Waltham, MA) according to the supplier protocols. Quantity and integrity of RNA samples were measured using NanoDrop ND-1000 UV-Vis Spectrophotometer and Agilent 2100 Bioanalyzer Lab-On-A-Chip Agilent 6000 Series II chip, respectively (7).

### RT and Quantitative PCR

RT for miR-205 was performed with 10 ng RNA per reaction using Taqman MicroRNA Reverse Transcription Kit (LifeTechnologies, Grand Island, NY). Quantitative PCR was performed on the ABI 7500 Real-Time PCR System with the following thermal cycles conditions: 50°C for 2 min, 95°C for 15 min, followed by 40 cycles of 95°C for 15 s and 60°C for 60 s. Changes in miR expression levels were normalized to small nucleolar RNA 234 (*sno234*) expression levels and analyzed by the  $\Delta\Delta C_T$  method. RT for mRNA was performed with 500 ng RNA per reaction using the Verso cDNA Synthesis Kit (LifeTechnologies) following the supplied protocol. Prior to RT, the RNA was DNase treated using the Turbo DNA-free kit (LifeTechnologies). Quantitative PCR was performed on the ABI 7500 Real-Time PCR System with the same cycling conditions described above. Changes in mRNA expression levels were normalized to glyceraldehyde-3-phosphate dehydrogenase expression levels and analyzed by the  $\Delta\Delta C_T$  method.

### miR ISH

ISH for miR-205 was performed using the miRCURY LNA microRNA ISH optimization kit 8 (Exiqon, Woburn, MA) according to manufacturer's protocol with the following modifications. Formalin-fixed tissue sections were incubated with 2.5  $\mu\text{g}/\text{ml}$  proteinase-K for 10 min at 37°C. *hsa-miR-205* and nonspecific (scramble) probes were used at a concentration of 200 nM and hybridized at 57°C for 1 h. After blocking, 1:1,400 dilution of the sheep anti-DIG-AP was applied to the tissue for 1 h at room temperature. The AP substrate reaction was carried out overnight in a humidity chamber at room temperature protected from light. For fluorescent detection, the following modifications were made. Scramble and miR-205 probe were used at either 200 nM or 400 nM and sheep anti-DIG-AP at 1:400. Vector Blue Alkaline Phosphatase (Vector Laboratories, Burlingame, CA) substrate kit was used according to manufacturer's protocol with the addition of 100 nm Levamisole. Substrate solution was replaced for several cycles of staining 20–30 min each, until color reaction was well developed.

### Immunohistochemistry

Formalin-fixed, paraffin-embedded tissue sections were deparaffinized through xylenes and ethanol series. The slides were pretreated with Proteinase-K (2.5  $\mu\text{g}/\text{ml}$ ) for 10 min at 37°C and/or antigen retrieval using sodium citrate buffer (10 nM Sodium Citrate, 0.05% Tween-20, pH 6.0) for 25 min in a pressure cooker. Hydrogen peroxide (3%), biotin block (ScyTek Laboratories, Logan, UT; BBK30), and Superblock (Fisher Scientific, 37580) pretreatments were performed. All antibodies were diluted in 5% Superblock in PBS. The following primary antibodies were incubated overnight at 4°C: anti-AQP2 (1:200, Santa Cruz Sc-9882) and anti-Vacuolar-type H<sup>+</sup>-ATPase (V-ATPase; 1:50, Santa Cruz sc-21209). The secondary antibodies that were used are UltraTek Anti-Polyvalent Biotinylated (ScyTek, ABN125) or UltraTek Anti-Goat Biotinylated Abs (ScyTek, AGL125AEC). Chromogen/Substrate Kit (ScyTek ACJ999) was used for color development for light microscopy. Fluorescent detection was performed after ISH and used a similar protocol starting from the Superblock pretreatment. The primary antibody for immunofluorescence was AQP3 (1:50, Alomone Labs AQP-003) and secondary antibody (Donkey anti-rabbit AlexaFlour 633) was used at 1:200 dilution for 1 h at room temperature in the dark. The slides were mounted with ProLong Diamond mounting media without DAPI (LifeTechnologies).

### Protein Isolation

Frozen mouse tissue was weighed and 10  $\mu\text{l}$  working buffer (62 mM Tris (pH 6.8), 2% sodium dodecyl sulfate, 10% Glycerol and 1 $\times$  Protease Inhibitor (ThermoFisher Scientific)) added per mg of tissue, followed by TissueLyser II (Qiagen USA) for 3–5 min.  $\beta$ -mercaptoethanol containing 0.04% bromophenol blue was added to a 5% final concentration. The samples were boiled for 5 min and centrifuged. Supernatant was transferred to a new tube and stored at  $-80^\circ\text{C}$ .

### Western Blot

Protein samples were heated at 95°C for 5 min and loaded onto Mini-Protein TGX Precast Gels (BioRad Laboratories, Hercules, CA) and electrophoresed using Tris-glycine-sodium dodecyl sulfate running buffer. Proteins were transferred to polyvinylidene fluoride (PVDF) membranes using standard transfer buffer (Tris-glycine with 20% methanol). Nonspecific binding was blocked using Superblock (Fisher Scientific, 37580) with 0.05% Tween-20 for 1 h at room temperature. Primary antibodies were incubated overnight at 4°C in 10% Superblock in PBS. Primary antibodies and dilutions were: *Cdc42* (1:2,000, Fisher Scientific PIPA1092) and *Cgn1* (1:1,000, Santa Cruz sc-377525). Glyceraldehyde-3-phosphate dehydrogenase (1:5,000, Santa Cruz sc-25778) or *Ku-70* (1:200, Santa Cruz sc-17789) was used as a control for loading and normalization. Membranes were washed with PBS-Tween and then incubated with either sheep anti-mouse HRP-Linked (1:5,000, Amersham NA931-1ML) or goat anti-rabbit HRP-Linked (1:5,000, Santa Cruz sc-2054) as appropriate. Chemiluminescent signal was developed using ECL Western Blotting Substrate (Pierce #32106).

### Imaging

Light micrographs and fluorescence images for **Figures 3–5** were obtained using a DMI4000 microscope equipped with a DFC450C digital camera and processed using the LAS-X software package (Leica Microsystems, Buffalo Grove, IL). Fluorescent images were captured in monochrome mode and digital color applied to facilitate merging of images. Images for **Figure 6** were captured on an Aperio Digital Scanner and processed using ImageScope software v.12.3 (Leica Microsystems).

### Statistical Analysis

Pairwise comparison of group means utilized the Wilcoxon rank-sum test. The statistical dependence between variables was measured by Spearman rank correlation with Bonferroni adjustment as appropriate for multiple comparisons. In all cases,  $\alpha = 0.05$  was set *a priori* as the threshold for statistical significance. All statistical tests were performed using Stata v.13.1 (StataCorp, College Station, TX).

## ACKNOWLEDGMENTS

The authors gratefully acknowledge the assistance of Jamie Mollett in the preparation of this manuscript.

## STATEMENT OF FINANCIAL SUPPORT

This work was supported by grant K08DK092340 from the National Institutes of Health/National Institute of Diabetes and Digestive and Kidney Disease (Bethesda, MD) to S.E.I. and by grant TL1RR025753 from the National Institutes of Health/National Center for Research Resources (Bethesda, MD) to S.E.I. through The Ohio State University Center for Clinical and Translational Science.

Disclosure: The authors have no conflicts of interest or financial disclosures related to this manuscript.

## REFERENCES

- Collins AJ, Foley R, Herzog C, et al. Excerpts from the United States Renal Data System 2007 annual data report. *Am J Kidney Dis* 2008;51(1 Suppl 1):S1–320.
- Ingraham SE, McHugh KM. Current perspectives on congenital obstructive nephropathy. *Pediatr Nephrol* 2011;26:1453–61.
- Miklovicova D, Cervenova O, Cernianska A, Jancovicova Z, Dedik L, Vasilenkova A. Long-term follow-up of renal function in patients after surgery for obstructive uropathy. *Pediatr Nephrol* 2008;23:937–45.
- Craven AM, Hawley CM, McDonald SP, Rosman JB, Brown FG, Johnson DW. Predictors of renal recovery in Australian and New Zealand end-stage renal failure patients treated with peritoneal dialysis. *Perit Dial Int* 2007;27:184–91.
- Ingraham SE, Saha M, Carpenter AR, et al. Pathogenesis of renal injury in the megabladder mouse: a genetic model of congenital obstructive nephropathy. *Pediatr Res* 2010;68:500–7.
- Singh S, Robinson M, Nahi F, et al. Identification of a unique transgenic mouse line that develops megabladder, obstructive uropathy, and renal dysfunction. *J Am Soc Nephrol* 2007;18:461–71.
- Becknell B, Carpenter AR, Allen JL, et al. Molecular basis of renal adaptation in a murine model of congenital obstructive nephropathy. *PLoS One* 2013;8:e72762.
- McHugh KM. Megabladder mouse model of congenital obstructive nephropathy: genetic etiology and renal adaptation. *Pediatr Nephrol* 2014;29:645–50.
- Akkina S, Becker BN. MicroRNAs in kidney function and disease. *Transl Res* 2011;157:236–40.
- Chandrasekaran K, Karolina DS, Sepsramaniam S, et al. Role of microRNAs in kidney homeostasis and disease. *Kidney Int* 2012;81:617–27.
- Li JY, Yong TY, Michael MZ, Gleadle JM. Review: The role of microRNAs in kidney disease. *Nephrology (Carlton)* 2010;15:599–608.
- Saal S, Harvey SJ. MicroRNAs and the kidney: coming of age. *Curr Opin Nephrol Hypertens* 2009;18:317–23.
- Orang AV, Safaralizadeh R, Hosseinpour Feizi MA. Insights into the diverse roles of miR-205 in human cancers. *Asian Pac J Cancer Prev* 2014;15:577–83.
- Paterson EL, Kolesnikoff N, Gregory PA, Bert AG, Khew-Goodall Y, Goodall GJ. The microRNA-200 family regulates epithelial to mesenchymal transition. *ScientificWorldJournal* 2008;8:901–4.
- Qin AY, Zhang XW, Liu L, et al. MiR-205 in cancer: an angel or a devil? *Eur J Cell Biol* 2013;92:54–60.
- Vosgha H, Salajegheh A, Smith RA, Lam AK. The important roles of miR-205 in normal physiology, cancers and as a potential therapeutic target. *Curr Cancer Drug Targets* 2014;14:621–37.
- Cai X, Xia Z, Zhang C, et al. Serum microRNAs levels in primary focal segmental glomerulosclerosis. *Pediatr Nephrol* 2013;28:1797–801.
- Wang G, Kwan BC, Lai FM, et al. Intrarenal expression of microRNAs in patients with IgA nephropathy. *Lab Invest* 2010;90:98–103.
- Wang G, Kwan BC, Lai FM, et al. Intrarenal expression of miRNAs in patients with hypertensive nephrosclerosis. *Am J Hypertens* 2010;23:78–84.
- Glowacki F, Savary G, Gnemmi V, et al. Increased circulating miR-21 levels are associated with kidney fibrosis. *PLoS One* 2013;8:e58014.
- Brown D, Hirsch S, Gluck S. Localization of a proton-pumping ATPase in rat kidney. *J Clin Invest* 1988;82:2114–26.
- Nielsen S, Kwon TH, Christensen BM, Promeneur D, Frøkiaer J, Marples D. Physiology and pathophysiology of renal aquaporins. *J Am Soc Nephrol* 1999;10:647–63.
- Chung PJ, Chi LM, Chen CL, et al. MicroRNA-205 targets tight junction-related proteins during urothelial cellular differentiation. *Mol Cell Proteomics* 2014;13:2321–36.
- Farmer DT, Shariat N, Park CY, Liu HJ, Mavropoulos A, McManus MT. Partially penetrant postnatal lethality of an epithelial specific microRNA in a mouse knockout. *PLoS One* 2013;8:e76634.
- Wang D, Zhang Z, O'Loughlin E, et al. MicroRNA-205 controls neonatal expansion of skin stem cells by modulating the PI(3)K pathway. *Nat Cell Biol* 2013;15:1153–63.
- Ben-Dov IZ, Tan YC, Morozov P, et al. Urine microRNA as potential biomarkers of autosomal dominant polycystic kidney disease progression: description of miRNA profiles at baseline. *PLoS One* 2014;9:e86856.
- Burbige KA, Lebowitz RL, Colodny AH, Bauer SB, Retik AB. The megacystis-megaureter syndrome. *J Urol* 1984;131:1133–6.
- WILLIAMS DI. Megacystis and megaureter in children. *Bull N Y Acad Med* 1959;35:317–27.
- Kwon TH, Frøkiaer J, Nielsen S. Regulation of aquaporin-2 in the kidney: a molecular mechanism of body-water homeostasis. *Kidney Res Clin Pract* 2013;32:96–102.
- Greene SB, Herschkowitz JI, Rosen JM. The ups and downs of miR-205: identifying the roles of miR-205 in mammary gland development and breast cancer. *RNA Biol* 2010;7:300–4.
- Ning MS, Andl T. Concise review: custodians of the transcriptome: how microRNAs guard stemness in squamous epithelia. *Stem Cells* 2015;33:1047–54.
- Kriebel S, Schmidt D, Holdenrieder S, et al. Analysis of tissue and serum microRNA expression in patients with upper urinary tract urothelial cancer. *PLoS One* 2015;10:e0117284.
- Tran MN, Choi W, Wszolek MF, et al. The p63 protein isoform  $\Delta Np63\alpha$  inhibits epithelial-mesenchymal transition in human bladder cancer cells: role of MIR-205. *J Biol Chem* 2013;288:3275–88.
- Tian C, Liu Q, Ma K, et al. Characterization of induced neural progenitors from skin fibroblasts by a novel combination of defined factors. *Sci Rep* 2013;3:1345.
- Muratsu-Ikeda S, Nangaku M, Ikeda Y, Tanaka T, Wada T, Inagi R. Down-regulation of miR-205 modulates cell susceptibility to oxidative and endoplasmic reticulum stresses in renal tubular cells. *PLoS One* 2012;7:e41462.
- Gandellini P, Profumo V, Casamichele A, et al. miR-205 regulates basement membrane deposition in human prostate: implications for cancer development. *Cell Death Differ* 2012;19:1750–60.
- Butt MJ, Tarantal AF, Jimenez DF, Matsell DG. Collecting duct epithelial-mesenchymal transition in fetal urinary tract obstruction. *Kidney Int* 2007;72:936–44.
- Brown D. Tight junctions: guardians of the paracellular pathway. *Kidney Int* 2000;57:2652–3.
- Hemmi A, Mori Y. Immunohistochemical study of cytokeratin distribution in the collecting duct of the human kidney. *Acta Pathol Jpn* 1991;41:516–20.
- Carpenter AR, Becknell B, Ingraham SE, McHugh KM. Ultrasound imaging of the murine kidney. *Methods Mol Biol* 2012;886:403–10.